

Article

Effect of Electrochemical Interaction between Chalcopyrite and Hexagonal Pyrrhotite on Flotation Separation

Tingsheng Qiu^{1,2}, Ce Zhang¹, Liu Yang¹, Jun Wang^{3,4}, Guanfei Zhao^{1,2}, Huashan Yan^{1,2,*}, Hao Wu¹, Xianhui Qiu^{1,2,*}, Baojun Yang^{3,4} and Rui Liao^{3,4}

¹ College of Resource and Environmental Engineering, Jiangxi University of Science and Technology, Ganzhou 341000, China; qiatingsheng@163.com (T.Q.); zly700507@163.com (C.Z.); yangliu999777@163.com (L.Y.); 9120220021@jxust.edu.cn (G.Z.); 18070476356@163.com (H.W.)

² Key Laboratory of Mining Engineering of Jiangxi Province, Jiangxi University of Science and Technology, Ganzhou 341000, China

³ School of Minerals Processing & Bioengineering, Central South University, Changsha 410017, China; wjwq2000@126.com (J.W.); yangbaojun0312@126.com (B.Y.); csuliaorui@163.com (R.L.)

⁴ Key Laboratory of Biohydrometallurgy of Ministry of Education, Changsha 410083, China

* Correspondence: jxustyhs@163.com (H.Y.); 9120140109@jxust.edu.cn (X.Q.); Tel.: +86-15297763712 (H.Y.); +86-15970795221 (X.Q.)

Abstract: The mechanism of electrochemical interaction between chalcopyrite and hexagonal pyrrhotite was analyzed via electrochemical interaction, copper ion concentration testing, and X-ray photoelectron spectroscopy (XPS) characterization. Besides, the effect of electrochemical interaction between the two minerals on the flotation separation was investigated using the mineral flotation tests, adsorption capacity tests, and a microcalorimetric test. Our research results showed that chalcopyrite had higher electrochemical activity than hexagonal pyrrhotite, and when the former acted as an anode during the electrochemical interaction of the two, the corrosion current density was three times higher than that when it acted alone, and the surface oxidation corrosion was intensified. At the same time, the interaction between the two minerals was accompanied by a large number of copper ions dissolved and adsorbed on the surface of the hexagonal pyrrhotite, so that adsorption of butyl xanthate intensified, adsorption increased, and flotation recovery increased by 5%–20%. However, owing to the increase in metal defects and the generation of hydrophilic sulfate, the surface of chalcopyrite hindered the adsorption of butyl xanthate on its surface, and the flotation recovery decreased by nearly 10% compared with that before the occurrence of the electrochemical interaction. This action also significantly weakened the inhibition effect of lime on hexagonal pyrrhotite and increased the difficulty of the flotation separation of the two minerals. The research results of this study provide theoretical guidance for the flotation separation of copper–sulfur ores containing pyrrhotite.

Keywords: chalcopyrite; hexagonal pyrrhotite; flotation separation; electrochemical interaction



Citation: Qiu, T.; Zhang, C.; Yang, L.; Wang, J.; Zhao, G.; Yan, H.; Wu, H.; Qiu, X.; Yang, B.; Liao, R. Effect of Electrochemical Interaction between Chalcopyrite and Hexagonal Pyrrhotite on Flotation Separation. *Minerals* **2023**, *13*, 1303. <https://doi.org/10.3390/min13101303>

Academic Editors: Bingqiao Yang, Weijun Peng, Shulei Li and Chiharu Tokoro

Received: 11 August 2023

Revised: 26 September 2023

Accepted: 5 October 2023

Published: 8 October 2023



Copyright: © 2023 by the authors. Licensee MDPI, Basel, Switzerland. This article is an open access article distributed under the terms and conditions of the Creative Commons Attribution (CC BY) license (<https://creativecommons.org/licenses/by/4.0/>).

1. Introduction

Copper is extensively used in electrical, construction, and defense applications because of its good ductility, and electrical and thermal conductivity. Chalcopyrite is an important copper-containing mineral that is often associated with pyrite, magnetite, and other sulfur–iron ores in natural deposits [1]. Flotation is generally utilized to achieve effective separation of chalcopyrite and associated sulfide iron ore due to the good hydrophobic properties of chalcopyrite [2,3]. However, with the continuous evolution of mineral resources into “poor, fine, and miscellaneous” resources, the flotation separation of chalcopyrite and associated sulfide iron ore in copper–sulfide ores has become increasingly difficult. This has made the study of copper–sulfur separation an important area of research in the field of mineral processing. For example, Zhang et al. [4] found that grinding with ceramic ball media is more favorable for the adsorption of the chalcopyrite surface on

the collector, and proposed a new way to enhance the flotation separation of chalcopyrite and pyrite by changing the grinding media. Jia et al. [5] synthesized thiohexanamide (THA) with good selectivity for chalcopyrite as a collector for the flotation separation of chalcopyrite from associated sulfide ores, which enhanced the chalcopyrite recovery index. Wei et al. [6] reported that polyaspartic acid (PAPA) had a good decreasing effect on thionite activated by copper ions. Khoso et al. [7] discovered that the novel innocuous reagent of polyglutamic acid (PGA) may interfere with the electrochemical activity between the collector and the surface of pyrrhotite, allowing effective copper–sulfur separation to be achieved. Zeng et al. [8] investigated the flotation separation mechanism of chalcopyrite and pyrrhotite, and found that butyl xanthate could oxidize on the surface of chalcopyrite to generate dixanthogen, while lime would depress the redox of butyl xanthate after forming a calcium film on the surface of pyrrhotite. Thus, the separation of the two minerals could be achieved under the highly alkaline condition of lime. In the above studies, scholars have conducted a lot of research on copper–sulfur flotation separation from the perspective of grinding media, flotation chemicals, and separation mechanisms; however, the intrinsic mechanism causing the difficulty in copper–sulfur separation in copper–sulfide ores is still unclear.

In nature, most metallic sulfide ores have semiconducting properties, and when different types of sulfide ores come into contact with each other in an electrolyte solution, they electrochemically interact and form a “primary cell” [9–11]. Minerals with a low surface electrostatic potential which are electrochemically active and act as anodes are presented in Equation (1), along with surface oxidative dissolution and the oxidation reaction. The mineral with a high surface electrostatic potential, which is electrochemically inert, functions as a cathode wherein oxygen is reduced on the surface, as shown in Equation (2) [12–14]. As the most common sulfide ore among metal sulfide ores, pyrite has significant electrochemical interactions with other copper, lead, and zinc sulfide ores, and affects the flotation separation of sulfur from copper, lead, and zinc to varying degrees [15–17]. For instance, Wu et al. [18] concluded that the electrochemical interaction between pyrite and chalcopyrite substantially promotes the oxidative dissolution on the surface of chalcopyrite, which causes the dissolved copper ions to be adsorbed on the surface of pyrite, thus it is unfavorable to the flotation separation of both minerals. Wang et al. [19] reported that the electrochemical interaction between pyrite and galena changed their surface composition and increased the difficulty of the flotation separation. Xia et al. [20] studied the effect of the electrochemical interaction between pyrite and copper-activated sphalerite on the flotation behavior of both minerals. Their results indicated that the electrochemical interaction contributed to the preferential adsorption of copper ions on the surface of sphalerite, while the surface of chalcopyrite could not easily adsorb butyl xanthate due to the generation of hydroxide; thus, the floatability was reduced. Qin et al. [21] found that the corrosion current of galena was four times higher than the self-corrosion current in the electrochemical interaction system of pyrite and galena, and the corrosion rate increased considerably. The electrochemical interaction also affected the generation of hydrophilic and hydrophobic products on the surface of both minerals, which decreased the floatability difference between them. In addition to pyrite, pyrrhotite is also a common type of pyrite, which is more susceptible to oxidation due to the defective crystal structure of pyrrhotite. Pyrite belongs to the equiaxial crystal system and has better oxidation resistance compared to pyrrhotite. This suggests that pyrrhotite is more difficult to separate from chalcopyrite than pyrite from chalcopyrite. The electrochemical interaction between pyrrhotite and chalcopyrite and its impact on the flotation separation has rarely been reported in the literature.



Based on the above literature, we took chalcopyrite and hexagonal pyrrhotite as the research object, and elaborated on the electrochemical interaction mechanism between

chalcopyrite and hexagonal pyrrhotite and its influence on the flotation separation through mineral flotation tests, adsorption capacity tests, copper ion concentration determination, and microcalorimetric tests, XPS tests, and electrochemical interactions. The results of our study provide theoretical guidance for the flotation separation of copper–sulfur ores containing pyrrhotite.

2. Materials and Methods

2.1. Test Materials

The chalcopyrite and hexagonal pyrrhotite samples used in the experiment were obtained from Daye, Hubei and Chifeng, Inner Mongolia, respectively. After preliminary crushing, the ores were manually picked to remove visible impurities. Then, they were dry ground by a ceramic ball mill and were sieved to obtain $-0.074\text{ mm} + 0.038\text{ mm}$ ore samples, which were placed in brown wide-mouth jars and stored in a refrigerator. A DX-2700 X-ray diffractometer from Dandong Fangyuan Instrument Co., Ltd., Dandong, China, was used for mineral phase analysis. Table 1 presents the results of the chemical analysis of chalcopyrite and hexagonal pyrrhotite samples, and the molar fraction of iron in the used pyrrhotite sample was calculated to be 47.72%, which was identified as hexagonal pyrrhotite [22]. The purity of chalcopyrite was 95.31%, and the purity of hexagonal pyrrhotites was 98.58% (Table 1). The X-Ray diffraction (XRD) results of the chalcopyrite and hexagonal pyrrhotite samples are shown in Figure 1. The XRD ray source comes from Cok, Dandong, China.

Table 1. Chemical analysis of mineral samples (%).

Minerals	Fe	S	Cu	Purity
Chalcopyrite	30.41	35.11	33.15	95.31
Hexagonal pyrrhotite	59.98	38.60	-	98.58

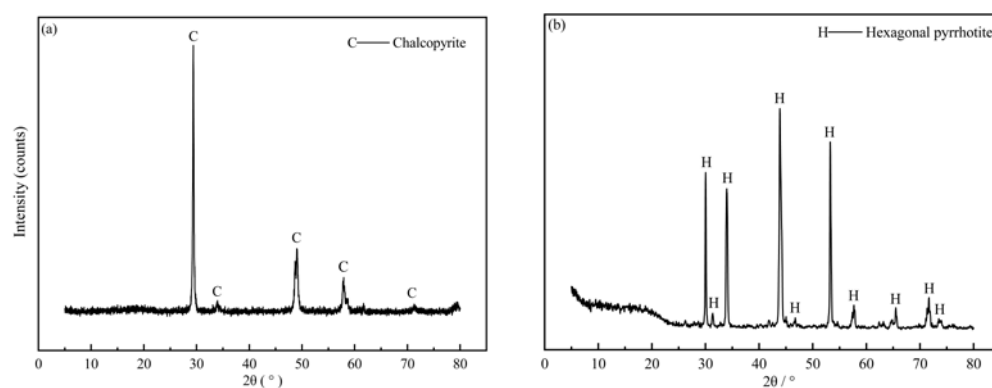


Figure 1. XRD results of (a) chalcopyrite; (b) hexagonal pyrrhotite samples.

Sodium hydroxide, hydrochloric acid, calcium oxide, potassium butyl xanthate, and methyl isobutyl methanol (MIBC) were the agents used in the tests, which were analytically pure, and the water used in the test was deionized water.

2.2. Research Methods

2.2.1. Electrochemical Interaction Test

The electrochemical behavior of minerals was studied using an Ametek-Princeton model PARSTAT 3000A-DX electrochemical workstation made in the USA. For the test, a saturated calomel electrode served as the reference electrode, a platinum sheet electrode served as the auxiliary electrode, a mineral electrode served as the working electrode, and a 0.01 mol/L KNO_3 solution served as the background electrolyte. A well-crystalline chalcopyrite/hexagonal pyrrhotite sample was cut into $1 \times 1 \times 1\text{ cm}$ cubic pieces, attached

with conductive glue with copper wire on each side, and sealed in the model with epoxy resin (Figure 2). The coupled electrodes were made from chalcopyrite and hexagonal pyrrhotite sheets that were glued together with conductive silver glue.

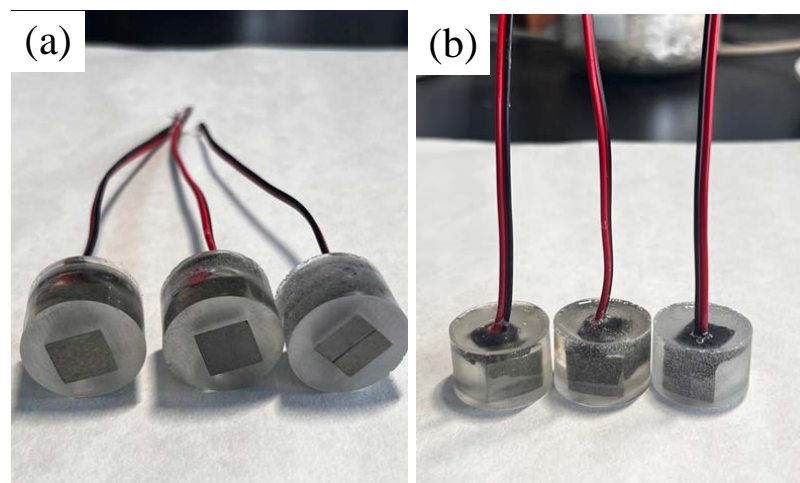


Figure 2. Sample drawing of the working electrode: (a) cross-sectional view of the sample; (b) front view of the sample.

Before each test, the surface of the working electrode was sanded step by step with 400 mm and 800 mm SiC emery papers and rinsed with deionized water. The polarization curve was scanned at a rate of 1 mV/s at an open circuit voltage of 250 mV. The corrosion voltage and current density can be calculated using a polarization curve. All potentials were converted to standard hydrogen electrode potentials for analysis.

2.2.2. Cu²⁺ Dissolution Test

Some 3 g of chalcopyrite was weighed and poured into a 50 mL conical flask, and hexagonal pyrrhotite was added to different conical flasks containing equal amounts of chalcopyrite in different ratios; then, 20 mL of deionized water was added to them, and they were sealed with a cling film skin band. Following stirring for 20 min, the filtrate was quickly filtered through a syringe with a filter tip to obtain filtrate 1 for reserve. Then, a 900-gauss magnetic block was used to separate the chalcopyrite from the hexagonal pyrrhotite in the filter residue. The obtained hexagonal pyrrhotite was placed in a 50 mL conical flask, 20 mL of hydrochloric acid solution with a concentration of 1 mol/L was added, the cling film skin band was closed and stirred for 20 min, and filtered filtrate 2 was kept as reserve.

The copper concentration in the filtrate 1 and filtrate 2 samples obtained from each set of tests was determined via a atomic absorption spectroscopy analysis. Filtrate 1 may represent the concentration of copper in solution after the electrochemical interaction between chalcopyrite and hexagonal pyrrhotite; filtrate 2 represents the concentration of copper adsorbed on the surface of hexagonal pyrrhotite after the electrochemical interaction. All experiments were repeated, and the average results are presented in the following.

2.2.3. XPS Test

In the analysis chamber of the X-ray photoelectron spectrometer, there is a vacuum of roughly 5×10^{-9} mbar, and the X-ray source is a monochromated AlK α source (Mono AlK α) with an operating voltage of 15 kV. The X-ray photoelectron spectrometer was manufactured in the USA by Thermo Scientific, Waltham, MA, USA, and is a K-Alpha+ device. After drying the specimen in a vacuum oven at 40 °C and weighing 2 g of the sample to be tested on an analytical scale, the specimen was flattened into a thin sheet with a grinder, and then subjected to XPS. The results of the test were then analyzed.

2.2.4. Mineral Flotation Test

In the experiment, the electrochemical process between the two minerals was simulated by mixing chalcopyrite and hexagonal pyrrhotite with equal masses and stirring in deionized water, and after 20 min of action, the chalcopyrite and hexagonal pyrrhotite were separated and set aside with a 900-gauss magnetic block.

The mineral flotation test was carried out in a 40 mL organic glass cell of an XFG-II flotation machine (Jilin Prospecting Machinery Factory, Jilin, China) as follows. Some 2 g of the mineral samples were weighed and poured into a clean beaker, and cleaned with an ultrasonic cleaner and placed in the flotation tank; then, about 40 mL of deionized water, was added, stirred well, and according to the test's requirements, a pH-adjusting agent, inhibitor, trapping agent, and frothing agent were added to the slurry in turn before the flotation test was performed. Finally, the resulting froth product and the product were filtered in the cell, dried, and weighed, and the flotation recovery was calculated using Equation (3). The test was repeated three times to obtain the average value.

$$R = \frac{m_1}{m_1 + m_2} \times 100\% \quad (3)$$

where R represents the flotation recovery of the mineral; m_1 denotes the mass of froth concentrate; and m_2 stands for the mass of tailings in the tank.

2.2.5. Adsorption Capacity Test

Mineral adsorption to butyl xanthate was measured using a PerkinElmer Lambda 35 UV spectrophotometer. Butyl xanthate solutions of various concentrations were produced, and their absorbance was measured at the characteristic wavelength of 300 nm. The acquired data were fitted to produce a standard curve for butylated xanthate concentration and absorbance (Figure 3). After weighing 2 g of the single mineral sample and cleaning it via ultrasonication, it was placed in a 50 mL conical flask with 40 mL of prepared aqueous solution of a different pH. Next, 20 mg/L of butyl xanthate solution was added, and the flask was sealed with a cling film skin band. The mixture was stirred for 20 min, and then left to stand before being centrifuged. Following clearance of the top transparent layer, another measurement of absorbance was performed, and this process was carried out three times for each point before calculating the average. The adsorption amount was calculated according to the following equation:

$$Q_t = \frac{(c_0 - c_t)V}{W} \quad (4)$$

where c_0 stands for the initial concentration of the butylated yellow solution (mg/L); c_t denotes the concentration of the butylated yellow solution in the supernatant at moment t (mg/L); W represents the weight of the mineral (g); and V signifies the volume of the butyl xanthate solution (L) corresponding to the adsorption amount Q_t (mg/g).

2.2.6. Microcalorimetric Test

The test equipment was a microcalorimetric calorimeter (model RD496-2000) from the Chinese Academy of Engineering Physics, which contained a calorimetric reaction cell and a reference reaction cell.

The procedure for preparing the calorimetric reaction cell was as follows. Weigh 0.03 g of mineral sample and 1 mL of deionized water and pour them into an outer glass tube; add 1.5 mL of a 15 mg/L butylated yellow solution to an inner glass tube, place the inner tube inside the outer tube, then place it into a stainless steel tube, cover with a perforated upper-end cap and secure it with a flexible stopper, insert a steel needle with a pressing handle, and spring through the hole in the upper-end cap into the inner glass tube; adjust the position of the steel needle with the pressed handle. Ultimately, the spring is inserted through the hole in the upper-end cap into the inner glass tube and adjusted. In the reference reaction cell, the outer glass tube is filled with 1 mL of deionized water,

and the inner glass tube is still filled with the same concentration of the butylated yellow solution, and the rest of the procedure is the same as that mentioned above.

The two prepared reaction cells were placed in the calorimetric furnace, the laboratory temperature was controlled at 25 °C, and the calorimetric parameters were set; after the curve stabilized, the steel pins of the two cells were pressed down simultaneously and quickly. At this point, the inner glass tubes in the two reaction cells were poked through and the adsorption reaction of the butylated yellow solution on the mineral surface began. The difference between the thermal effects of the two reaction cells was transformed by the measuring and control instrument into an electrical signal that was recorded by the computer and presented as a calorimetric curve.

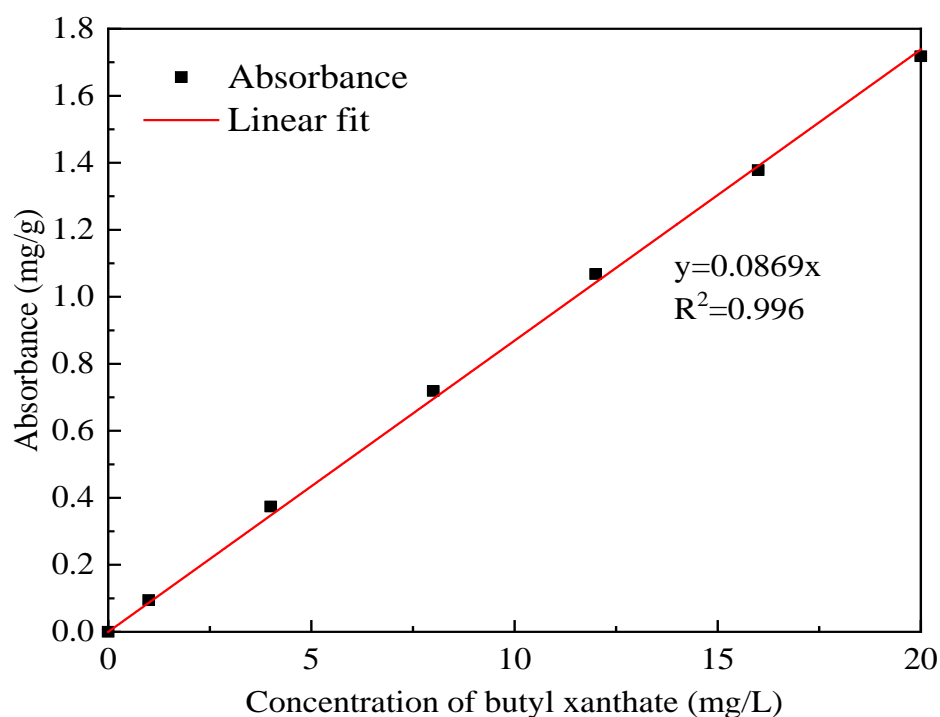


Figure 3. Adsorption standard curve of butyl xanthate.

3. Results and Discussion

3.1. Electrochemical Behavior Studies

3.1.1. Open Circuit Potential Measurement

The electrochemical interaction between the sulfide ores was closely related to the open circuit potential of the mineral electrode surfaces. Figure 4 displays the results of the open circuit potential tests of chalcopyrite and hexagonal pyrrhotite in natural pH aqueous solutions.

As can be observed, the open circuit potentials of chalcopyrite and hexagonal pyrrhotite were 101.22 mV and 208.26 mV, respectively, at equilibrium, with chalcopyrite having a much lower open circuit potential than hexagonal pyrrhotite. Therefore, chalcopyrite was electrochemically active as the anode, and hexagonal pyrrhotite was electrochemically inert as the cathode when the two interacted electrochemically.

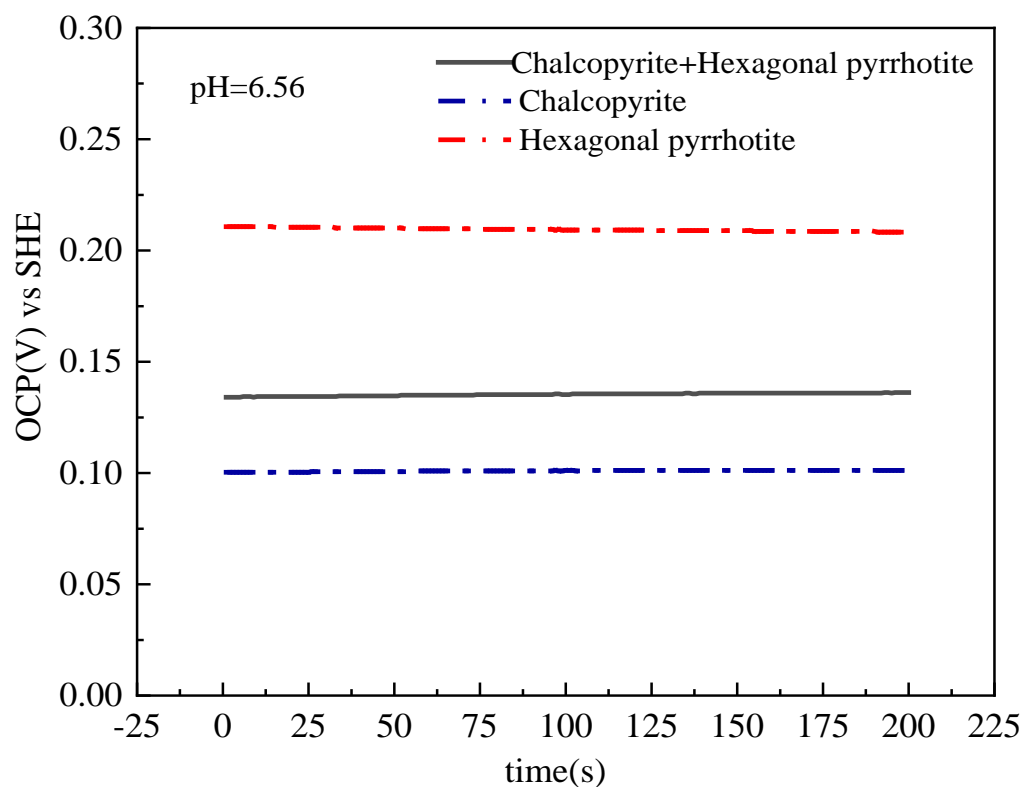


Figure 4. Open circuit potentials of chalcopyrite and hexagonal pyrrhotite.

3.1.2. Polarization Curve Measurement

The kinetic potential polarization curve provides information about the corrosion voltage and corrosion current density of the electrode material under test, where the corrosion current density characterizes the speed of the corrosion reaction of the electrode material. Figure 5 illustrates the polarization curves of chalcopyrite and hexagonal pyrrhotite before and after electrocoupling, and fitting the data in Figure 5 yields the results presented in Table 2.

Table 2. Polarization curve-related fitting parameters.

Electrodes	Hexagonal Pyrrhotite	Chalcopyrite	Coupled Electrode
Corrosion current density ($\mu\text{A}/\text{cm}^2$)	3.13	0.44	1.51

According to the analysis of Mu et al. [23], the corrosion process of the anode is mainly influenced by the oxidation and dissolution of minerals during the polarization process, while the corrosion process of the cathode is mostly manifested by the reduction of dissolved oxygen on the surface of minerals. It can be observed in Table 2 that the corrosion current density of the chalcopyrite single mineral electrode is $0.44 \mu\text{A}/\text{cm}^2$, and the corrosion current density of the chalcopyrite increases from $0.44 \mu\text{A}/\text{cm}^2$ to $1.51 \mu\text{A}/\text{cm}^2$ when chalcopyrite is coupled with hexagonal pyrrhotite. The results demonstrated that chalcopyrite was more active, and the oxidative corrosion rate was accelerated after electrochemical interaction with hexagonal pyrrhotite.

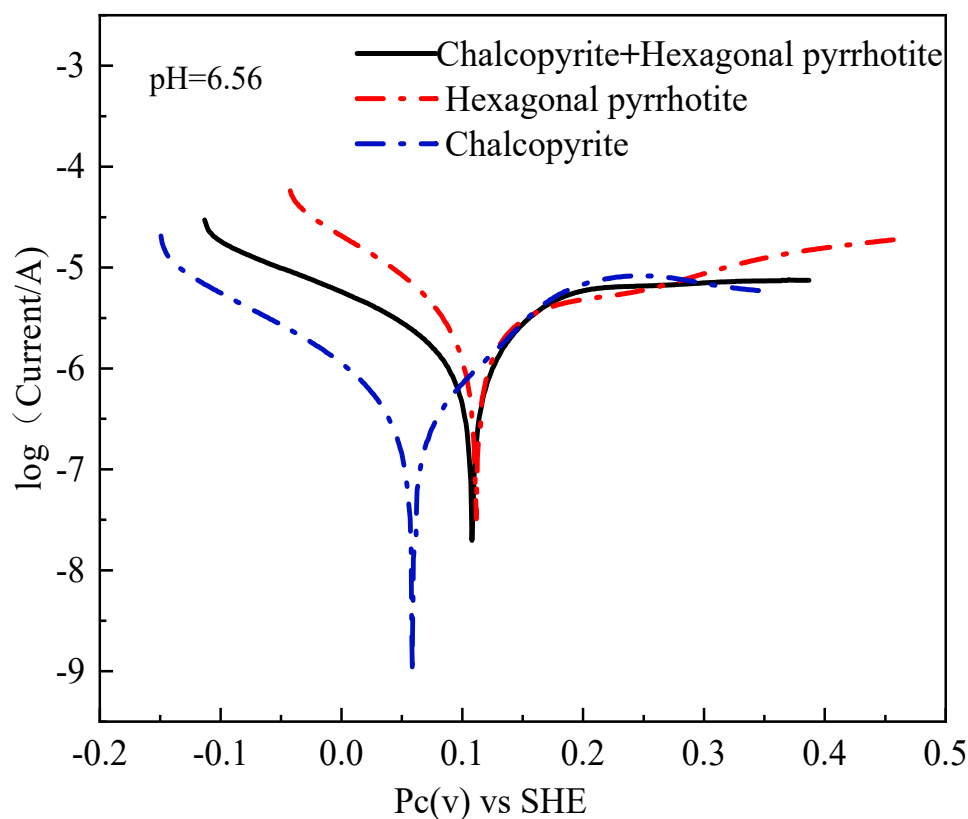


Figure 5. Polarization curves of chalcopyrite and hexagonal pyrrhotite before and after electrocoupling.

3.2. Cu^{2+} Dissolution Test Analysis

The interaction between the two minerals is often accompanied by the dissolution of metal ions from the mineral surface, and the dissolved metal ions play an important role in the activation and inhibition of the minerals. In systems wherein chalcopyrite is present, the dissolution of copper ions is an inevitable phenomenon. Therefore, the effect of the presence of chalcopyrite and hexagonal pyrrhotite in different ratios on the dissolution of copper ions from the surface of chalcopyrite was investigated; the concentrations of copper ions in solution and those adsorbed on the surface of hexagonal pyrrhotite were tested separately, and the test results are exhibited in Figure 6. The total amount of copper ions in the graph is the sum of the two.

The total amount of copper ions dissolved on the surface of chalcopyrite was only 0.09 mg/g in the absence of hexagonal pyrrhotite; in the presence of hexagonal pyrrhotite, when its content increased from 0.1 g to 3 g, the total amount of dissolved copper ions was 0.13, 0.21, 0.43, and 0.63 mg/g⁻¹, respectively. The presence of hexagonal pyrrhotite greatly promoted the dissolution of copper ions on the surface, and its dissolution amount was positively correlated with the content of hexagonal pyrrhotite. It is worth mentioning that as the content of hexagonal pyrrhotite increased, the copper ion content in the slurry solution showed a decreasing trend. When the ratio reached 1:1, the concentration of copper ions in the slurry solution was as low as 0.005 mg/g⁻¹, while that of the copper ions adsorbed on the surface of hexagonal pyrrhotite was as high as 0.625 mg/g⁻¹. It can be concluded that when the two interacted, the dissolved copper ions were primarily adsorbed on the surface of the hexagonal pyrrhotite, and they had an activating effect on it, while the free copper ions in the slurry were fewer.

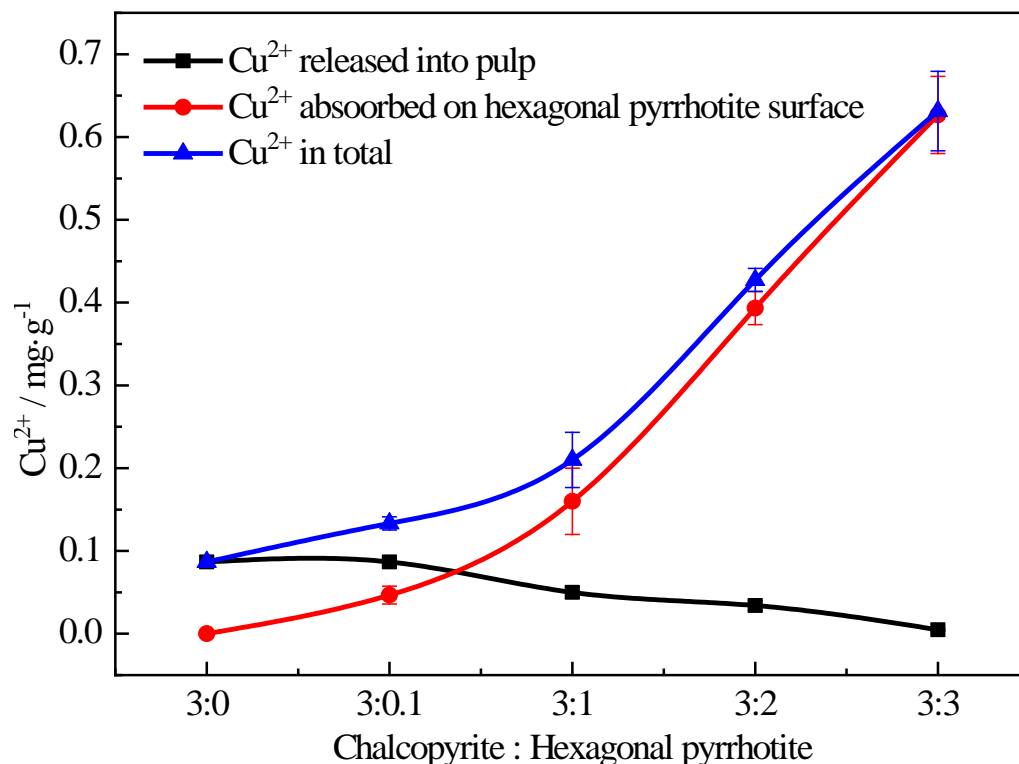


Figure 6. Dissolution of copper ions on the surface of chalcopyrite under different proportioning conditions.

3.3. XPS Analysis of Mineral Surfaces

To investigate the impact of electrochemistry on the surface properties of chalcopyrite and hexagonal pyrrhotite, XPS measurements were carried out to analyze the changes in the surface properties of chalcopyrite and hexagonal pyrrhotite before and after electrochemical treatment.

Table 3 presents the changes in elemental concentrations and atomic ratios on the surface of chalcopyrite and hexagonal pyrrhotite before and after electrochemistry. The table shows that copper was detected on the surface of hexagonal pyrrhotite after the reaction with chalcopyrite at a concentration of 1.24%. A faint Cu 2p peak near a binding energy of 931 eV can be observed on the hexagonal pyrrhotite surface after the reaction in Figure 7. This indicates that copper ions are adsorbed on the surface of the hexagonal pyrrhotite after electrochemical action, which is consistent with the results of the copper ion dissolution test. At the same time, the Fe/S on the surface of hexagonal pyrrhotite increased from 0.85 to 0.92 after the electrochemical action, and the mineral surface was sulfur-rich compared to the pre-action state. Besides, the S 2p peak on the surface of hexagonal pyrrhotite was significantly enhanced after the interaction (see Figure 7). The S element concentration on the surface of hexagonal pyrrhotite increased from 11.83% to 16.2% after the interaction (see Table 3). Combined with the activation effect of copper ions, it is speculated that hexagonal pyrrhotite may have generated and adsorbed CuS on its surface after interaction with chalcopyrite. This increased its hydrophobicity [24]. At the same time, the surface of chalcopyrite may suffer from metal ion defects due to the solubilization of copper ions, which affects its adsorption to the capture agent [18].

Table 3. Surface element concentrations and atomic ratios of chalcopyrite and hexagonal pyrrhotite.

Specimens	Elemental Concentration (%)					Atomic Ratio
	C	O	Cu	Fe	S	
Chalcopyrite	22.85	24.41	14.36	13.76	24.62	Cu/Fe/S = 1/0.96/1.71
Chalcopyrite (after)	24.09	27.06	12.79	12.68	23.38	Cu/Fe/S = 1/0.99/1.82
Hexagonal pyrrhotite	25.45	48.91	\	13.82	11.83	Fe/S = 1/0.85
Hexagonal pyrrhotite (after)	24.39	40.07	1.24	17.55	16.2	Fe/S = 1/0.92

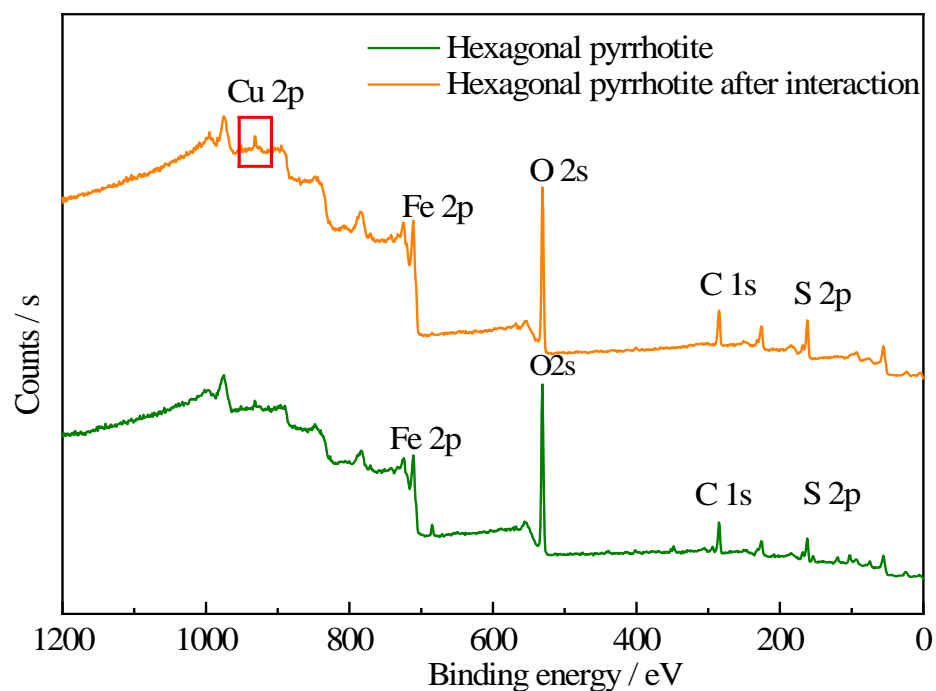
**Figure 7.** Full-spectrum scanning spectrum of hexagonal pyrrhotite surface.

Figure 8a,b present the fine profiles of Cu 2p and S 2p before and after the surface action of chalcopyrite, respectively. In this case, samples A and B are chalcopyrite before and chalcopyrite after the electrochemical action, respectively. In Figure 8a, the Cu 2p fine spectrum shows no satellite peaks around 942 eV, indicating that the copper of chalcopyrite is present as monovalent copper (Cu^+), and the peaks appearing at 932.4 eV and 952.2 eV are consistent with the Cu 2p peaks of chalcopyrite tested in the other literature [25,26]. It is easy to see that the Cu 2p peaks of chalcopyrite did not change before and after the interaction, demonstrating that the interaction with hexagonal pyrrhotite did not change the environment and state of Cu that was present on the surface of chalcopyrite. Figure 8b) shows that the S 2p peak on the chalcopyrite surface is fitted by four main peaks. Among them, the peak near 161.4 eV is the peak of monosulfide (S^{2-}), the peak near 162.5 eV is the peak of disulfide (S_2^{2-}), the peak near 163.2 eV is the peak of polysulfide (S_n^{2-}), and the peak near 169.3 eV is the peak of sulfate (SO_4^{2-}) [27–30]. Meanwhile, the peak area of sulfate on the surface of chalcopyrite was slightly enhanced after the interaction, proving once again that the addition of hexagonal pyrrhotite promoted the oxidation of the chalcopyrite surface. Figure 9 displays the inferred electrochemical interaction model between chalcopyrite and hexagonal pyrrhotite.

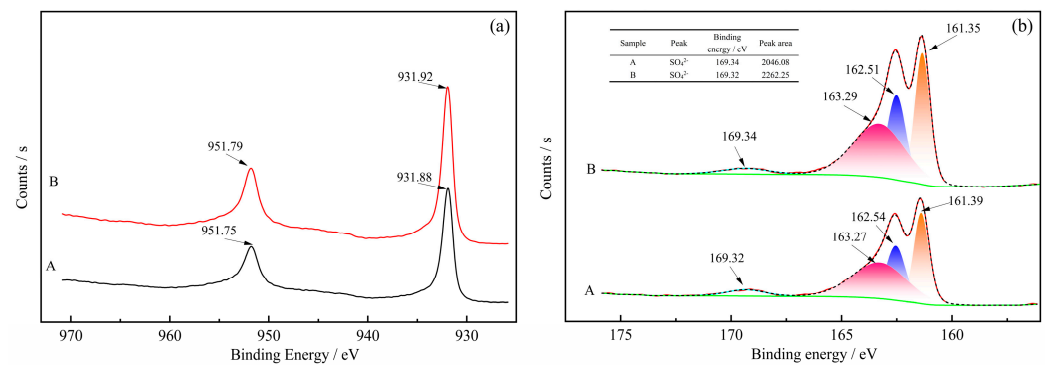


Figure 8. Scanning spectra of Cu 2p (a) and S 2p (b) on the chalcopyrite surface.

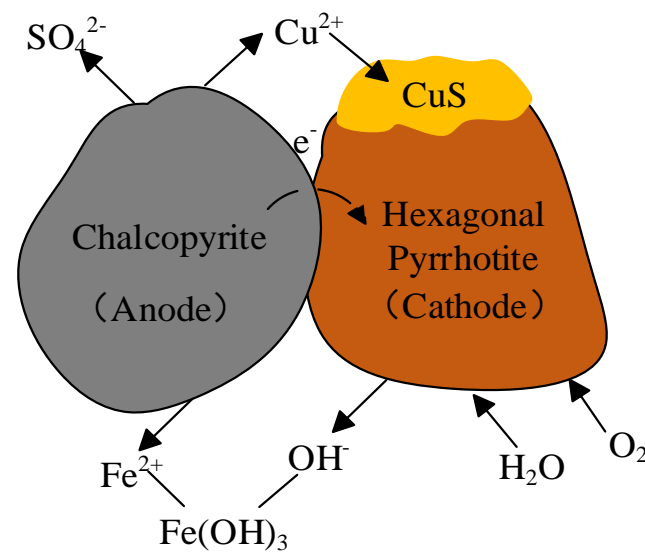


Figure 9. Modelling of the electrochemical interaction between chalcopyrite and hexagonal pyrrhotite.

3.4. Mineral Flotation Behavior

To find out the effect of the above electrochemical interactions on the flotation separation of the two minerals, flotation tests were conducted at different pH conditions using 15 mg/L butyl xanthan as a trapping agent and 15 mg/L MIBC as a foaming agent. The flotation recoveries of chalcopyrite and hexagonal pyrrhotite, which underwent electrochemical interactions, varied depending on the pH value of the slurry (Figure 10).

The flotation recoveries of chalcopyrite before the electrochemical action were around 90% higher than those of hexagonal pyrrhotite within the pulp pH examined, and the difference in flotation recoveries between the two was up to 53%. After the electrochemical action, the flotation behavior of both minerals changed considerably compared to before the occurrence of the electrochemical action. Throughout the flotation pH, the flotation recovery of chalcopyrite after the electrochemical action decreased by nearly 10% compared to before the action, while the flotation of hexagonal pyrrhotite was significantly improved, with recoveries increasing by 5%–20%. Compared to before the occurrence of the electrochemical action, the gap between the floatability of the two minerals was substantially decreased, with the maximum difference in flotation recovery decreasing by approximately 22%.

Lime is commonly employed to suppress sulfide iron ore in the flotation process of sulfide ores to achieve copper–sulfur separation [31]. Therefore, lime addition was investigated for its effect on chalcopyrite and hexagonal pyrrhotite flotation behavior before and after electrochemical treatment (condition: 15 mg/L BX and 15 mg/L MIBC). The experimental results are shown in Figure 11.

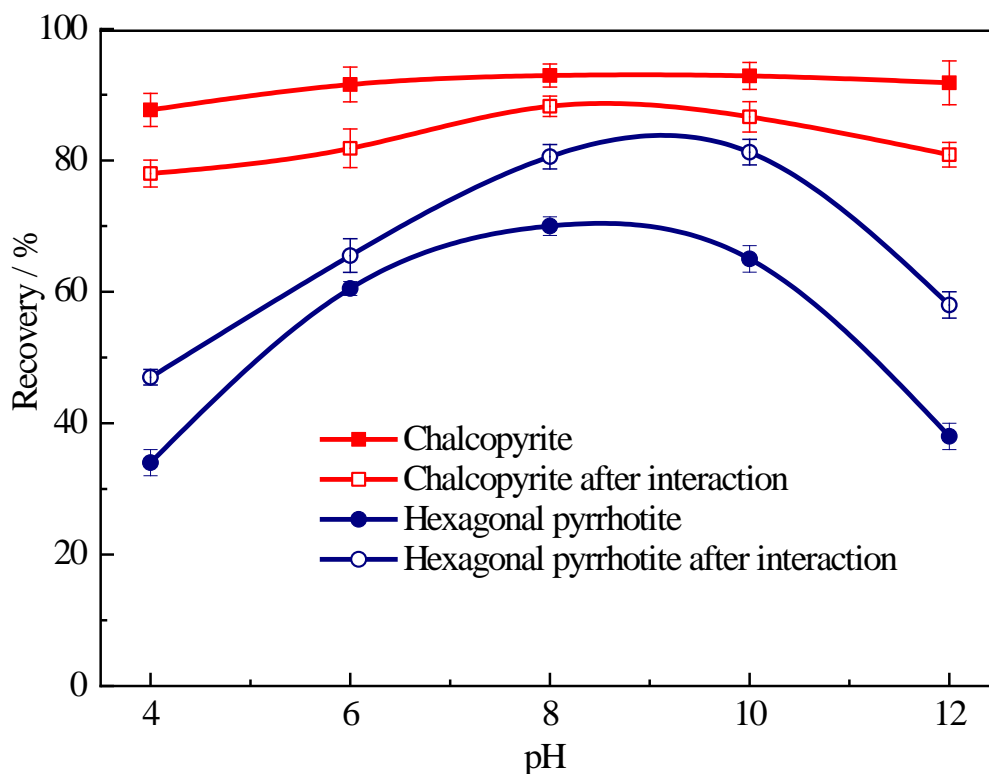


Figure 10. Effect of pulp pH on the flotation behavior of chalcopyrite and hexagonal pyrrhotite.

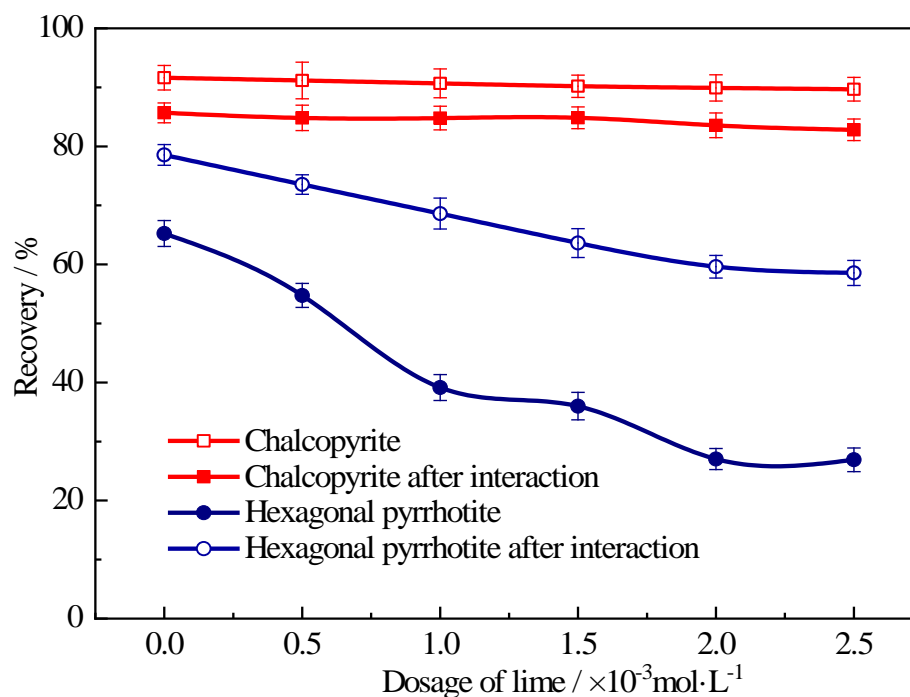


Figure 11. Effect of lime dosage on the flotation behavior of chalcopyrite and hexagonal pyrrhotite.

In Figure 11, it can be observed the recovery of chalcopyrite before the electrochemical action was maintained at around 90%, which was unaffected by the concentration of lime. However, with the increase in lime dosage, the recovery of hexagonal pyrrhotite decreased from 65.25% to 26.91%, showing a more obvious downward trend. This may be attributed to the fact that the orbital coefficients of Fe atoms in the HOMO orbitals of hexagonal pyrrhotite are much larger than those of S atoms, and the electron acceptor

$\text{Ca}(\text{OH})^+$ is more likely to react with the negatively charged nucleophilic HOMO orbitals, resulting in the generation of a large number of hydrophilic substances such as $\text{Ca}(\text{OH})_2$ and CaSO_4 on the surface of hexagonal pyrrhotite [32]. The flotation of chalcopyrite was slightly reduced after the electrochemical action, and the recovery decreased by nearly 5%, while the flotation of hexagonal pyrrhotite increased significantly, and the flotation recovery increased from 13% to 32%. This may be due to the fact that Cu^{2+} dissolved from chalcopyrite generates a hydrophobic film of CuS on the surface of hexagonal pyrrhotite, which leads to the better floatability of hexagonal pyrrhotite, in agreement with the reaction model presented in Figure 9. The difference in flotation characteristics was decreased, and the greatest difference in flotation recovery was lowered from 63% before the action to 24% after the action, making the flotation separation more difficult. It is evident that when the lime dose was increased, the recovery of hexagonal pyrrhotite decreased after the action, although the degree of the loss was significantly less than before the action. This indicates that it is more difficult to inhibit hexagonal pyrrhotite using lime after the interaction with chalcopyrite.

3.5. Analysis of Butyl Xanthate Adsorption on Mineral Surfaces

The strength and ease of the adsorption of the trapping agent to the target minerals is critical to effective mineral recovery. The changes in the adsorption capacity of butyl xanthate via chalcopyrite and hexagonal pyrrhotite before and after the electrochemical action under different pH conditions were determined separately using a UV spectrophotometer. The experimental results are displayed in Figure 12.

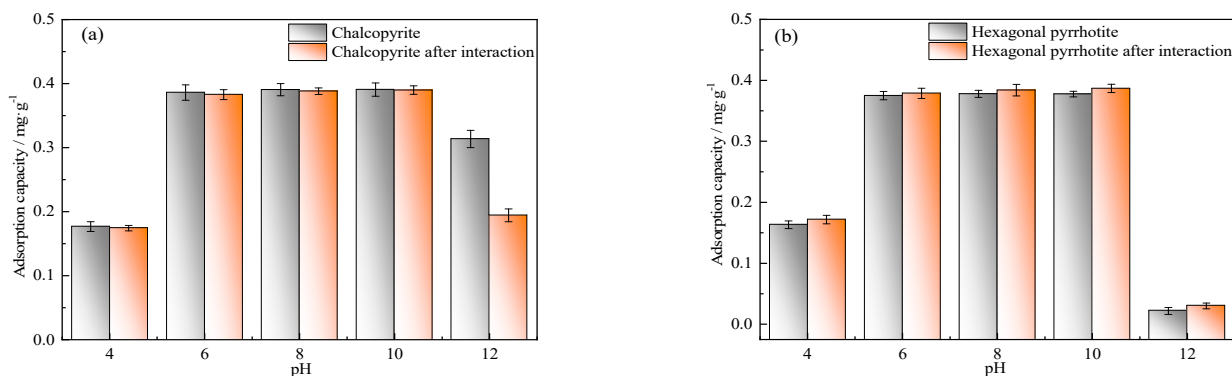


Figure 12. Adsorption of butyl xanthate on the surface of chalcopyrite (a) and hexagonal pyrrhotite (b) as a function of pulp pH.

The adsorption of butyl xanthate by both chalcopyrite and hexagonal pyrrhotite showed a trend of increasing and then decreasing over the examined pH range (Figure 12). The adsorption amounts were weaker in acidic and stronger in alkaline environments, while the adsorption amounts were larger in neutral and weakly alkaline environments, which were in general agreement with the flotation results. Figure 12a exhibits a slight decrease in the adsorption capacity of chalcopyrite for butyl xanthate after the electrochemical interaction of chalcopyrite with hexagonal pyrrhotite. And under alkaline conditions, the butyl xanthate adsorption on chalcopyrite dropped substantially from 0.313 mg/g^{-1} to 0.194 mg/g^{-1} , which may originate from the fact that strong alkaline conditions are more likely to form hydrophilic hydroxide films on the surface of chalcopyrite and hinder the subsequent butyl xanthate adsorption on its surface. The adsorption of butylated xanthate by hexagonal pyrrhotite showed different degrees of increase after the electrochemical action under different pH conditions (Figure 12b).

3.6. Thermodynamic Analysis of Butyl Xanthate Adsorption on Mineral Surfaces

The calorimetric curves of the butyl xanthate absorption process on the surfaces of chalcopyrite and hexagonal pyrrhotite before and after electrochemical action were recorded

separately using a microcalorimeter (Figure 13), and the mechanism of the change in flotation behavior following the interaction between chalcopyrite and hexagonal pyrrhotite was investigated from a thermodynamic point of view.

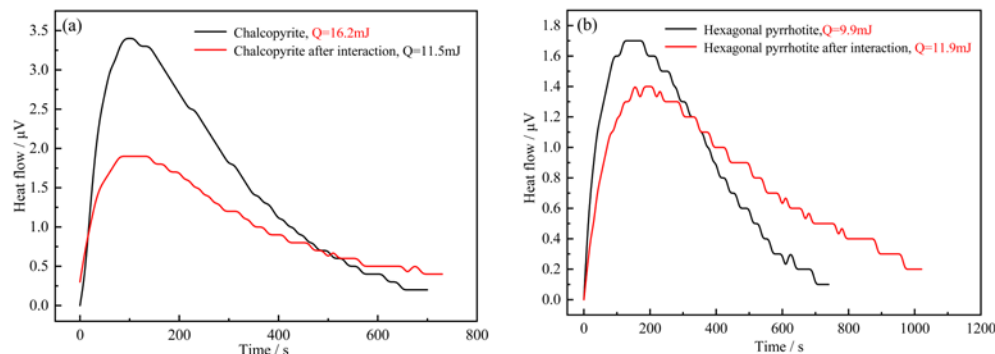


Figure 13. Calorimetric curves of the adsorption of butyl xanthate on the surface of chalcopyrite (a) and hexagonal pyrrhotite (b).

Figure 13 displays that the calorimetric curves for the adsorption of the agents on the surface of chalcopyrite and hexagonal pyrrhotite are both positive, indicating that the butyl xanthate adsorption on the surface of both minerals is an exothermic process [33]. The heat of the adsorption of butyl xanthate on the surface of chalcopyrite after the electrochemical action was 4.7 mJ lower than that before the action (Figure 13a)), and the thermal effect was reduced, suggesting that the extent of the reaction was weakened. The heat release of butyl xanthate adsorption on the surface of hexagonal pyrrhotite was only 9.9 mJ (Figure 13b)), indicating that the reaction was very weak, while the heat of adsorption of butyl xanthate on hexagonal pyrrhotite after the action increased to 11.9 mJ, demonstrating that the adsorption of butyl xanthate on hexagonal pyrrhotite after the action was more complete, and the reaction was more violent.

4. Conclusions

- (1) The surface electrostatic potential of chalcopyrite was smaller than that of hexagonal pyrrhotite, so that when the electrochemical interaction occurred, chalcopyrite was electrochemically active as the anode. When the two minerals were in electrochemical contact, the surface corrosion current density on the surface of chalcopyrite increased from $0.44 \mu\text{A}/\text{cm}^2$ to $1.51 \mu\text{A}/\text{cm}^2$, and the surface oxidation corrosion was aggravated.
- (2) The analysis of mineral surface properties showed that after the electrochemical action, the surface of chalcopyrite accelerated oxidation and dissolution, and a large number of copper ions were dissolved and adsorbed on the surface of hexagonal pyrrhotite; meanwhile, the adsorption sites of its metal ions were reduced, and part of the hydrophilic sulfate was generated.
- (3) The results of the mineral flotation and adsorption tests demonstrated that after the electrochemical action, the degree of adsorption reaction between the surface of the chalcopyrite and butyl xanthan was weakened, and the adsorption amount decreased; the adsorption reaction on the surface of the hexagonal pyrrhotite intensified, and the adsorption amount increased. Furthermore, the floatability gap between the two minerals was decreased, and it was difficult to accomplish the separation by adding a large amount of lime.

Author Contributions: Conceptualization, T.Q.; methodology, C.Z.; validation, L.Y., H.W. and G.Z.; formal analysis, B.Y.; resources, B.Y.; data curation, R.L.; writing—original draft preparation, C.Z.; writing—review and editing, H.Y. and L.Y.; visualization, X.Q.; supervision, H.Y.; project administration, J.W.; funding acquisition, H.Y. All authors have read and agreed to the published version of the manuscript.

Funding: This work was supported by the National Key R&D Program Project (No. 2022YFC2904501), the National Natural Science Foundation of China (No. 51974138), the Cultivation of Reserve Projects for National Science and Technology Awards in Jiangxi Province (20212AEI91009), and the Doctoral Research Foundation of Jiangxi University of Science and Technology (No. 205200100631).

Data Availability Statement: Not applicable.

Acknowledgments: The authors gratefully acknowledge the Laboratory of Resource and Environmental Engineering of Jiangxi University of Science and Technology, for providing the experimental conditions. The authors gratefully acknowledge Ke Zhang, Yang Liu, Hongchang Liu and Min Gan for their guidance during the electrochemical testing experiments.

Conflicts of Interest: The authors declare no conflict of interest.

References

1. Yang, S.; Tang, X.; Chen, R.; Fan, X.; Miao, J.; Luo, X. Application of Maleic Acid–Acrylic Acid Copolymer as an Eco-Friendly Depressant for Effective Flotation Separation of Chalcopyrite and Galena. *Minerals* **2023**, *13*, 191.
2. Liu, C.H.; Fan, F.Y.; Liu, Q.Y. Copper Resources Supply and Consumption Patterns and Trend in the Belt and Road Region. *Conserv. Util. Miner. Resour.* **2018**, *2*, 44–51.
3. Han, G.; Wen, S.; Wang, H.; Feng, Q. Interaction mechanism of tannic acid with pyrite surfaces and its response to flotation separation of chalcopyrite from pyrite in a low-alkaline medium. *J. Mater. Res. Technol.* **2020**, *9*, 4421–4430.
4. Zhang, X.; Qin, Y.; Han, Y.; Li, Y.; Gao, P.; Li, G.; Wang, S. A potential ceramic ball grinding medium for optimizing flotation separation of chalcopyrite and pyrite. *Powder Technol.* **2021**, *392*, 167–178. [[CrossRef](#)]
5. Jia, Y.; Huang, K.; Wang, S.; Cao, Z.; Zhong, H. The selective flotation behavior and adsorption mechanism of thiohexanamide to chalcopyrite. *Miner. Eng.* **2019**, *137*, 187–199.
6. Wei, Q.; Jiao, F.; Dong, L.Y.; Liu, X.D.; Qin, W.Q. Selective depression of copper-activated sphalerite by polyaspartic acid during chalcopyrite flotation. *Trans. Nonferrous Met. Soc. China* **2021**, *31*, 1784–1795.
7. Khoso, S.A.; Gao, Z.; Meng, X.; Hu, Y.; Sun, W. The depression and adsorption mechanism of polyglutamic acid on chalcopyrite and pyrrhotite flotation systems. *Minerals* **2019**, *9*, 510. [[CrossRef](#)]
8. Zeng, W.N.; Ren, L.Y.; Cao, Y.; Zeng, S.L. Study on Mechanism of Action of Xanthate in Flotation Separation of Chalcopyrite and Pyrrhotite. *Non-Ferrous Met. Benefic. Part* **2020**, *6*, 30–35.
9. Nowak, P.; Krauss, E.; Pomianowski, A. The electrochemical characteristics of the galvanic corrosion of sulphide minerals in short-circuited model galvanic cells. *Hydrometallurgy* **1984**, *12*, 95–110. [[CrossRef](#)]
10. Cheng, X.; Iwasaki, I. Pulp potential and its implications to sulfide flotation. *Miner. Proc. Ext. Met. Rev.* **1992**, *11*, 187–210. [[CrossRef](#)]
11. Zhang, Y.; Hu, Y.; Wang, L.; Sun, W. Systematic review of lithium extraction from salt-lake brines via precipitation approaches. *Miner. Eng.* **2019**, *139*, 105868.
12. Ekmekçi, Z.; Demirel, H. Effects of galvanic interaction on collectorless flotation behaviour of chalcopyrite and pyrite. *Int. J. Miner. Process.* **1997**, *52*, 31–48. [[CrossRef](#)]
13. Liu, Q.; Li, H.; Zhou, L. Galvanic interactions between metal sulfide minerals in a flowing system: Implications for mines environmental restoration. *Appl. Geochem.* **2008**, *23*, 2316–2323. [[CrossRef](#)]
14. Owusu, C.; Addai-Mensah, J.; Fornasiero, D.; Zanin, M. Estimating the electrochemical reactivity of pyrite ores—their impact on pulp chemistry and chalcopyrite flotation behaviour. *Adv. Powder Technol.* **2013**, *24*, 801–809. [[CrossRef](#)]
15. Qin, W.; Wang, X.; Ma, L.; Jiao, F.; Liu, R.; Yang, C.; Gao, K. Electrochemical characteristics and collectorless flotation behavior of galena: With and without the presence of pyrite. *Miner. Eng.* **2015**, *74*, 99–104. [[CrossRef](#)]
16. Yang, B.; Tong, X.; Lan, Z.; Cui, Y.; Xie, X. Influence of the Interaction between Sphalerite and Pyrite on the Copper Activation of Sphalerite. *Minerals* **2018**, *8*, 16. [[CrossRef](#)]
17. Zhang, X.; Han, Y.; Gao, P.; Li, Y. Effects of grinding media on grinding products and flotation performance of chalcopyrite. *Miner. Eng.* **2020**, *145*, 106070. [[CrossRef](#)]
18. Wu, J.; Ma, W.; Wang, X.; Jiao, F.; Qin, W. The effect of galvanic interaction between chalcopyrite and pyrite on the surface chemistry and collector adsorption: Flotation and DFT study. *Colloids Surf. A* **2020**, *607*, 125377. [[CrossRef](#)]
19. Wang, X.; Qin, W.; Jiao, F.; Wu, J. The influence of galvanic interaction on the dissolution and surface composition of galena and pyrite in flotation system. *Miner. Eng.* **2020**, *156*, 106525. [[CrossRef](#)]
20. Xia, L.; Hart, B.; Larachi, F.; Gravel, O. Galvanic interaction of pyrite with Cu activated sphalerite and its effect on xanthate adsorption. *Can. J. Chem. Eng.* **2019**, *97*, 2671–2677. [[CrossRef](#)]
21. Qin, W.Q.; Wang, X.J.; Ma, L.Y.; Jiao, F.; Liu, R.Z.; Gao, K. Effects of galvanic interaction between galena and pyrite on their flotation in the presence of butyl xanthate. *Trans. Nonferrous Met. Soc. China* **2015**, *25*, 3111–3118. [[CrossRef](#)]
22. Liang, D.Y.; He, G.W.; Zou, N. The isomeromorphism of pyrrhotite and its Treatment featuredifferentia. *J. Guangdong Non Ferr. Met.* **1997**, *1*, 1–5.

23. Mu, Y.; Peng, Y.; Lauten, R.A. The galvanic interaction between chalcopyrite and pyrite in the presence of lignosulfonate-based biopolymers and its effects on flotation performance. *Miner. Eng.* **2018**, *122*, 91–98. [[CrossRef](#)]
24. Buswell, A.; Nicol, M. Some aspects of the electrochemistry of the flotation of pyrrhotite. *J. Appl. Electrochem.* **2002**, *32*, 1321–1329. [[CrossRef](#)]
25. Yin, M.; Wu, C.-K.; Lou, Y.; Burda, C.; Koberstein, J.T.; Zhu, Y.; O'Brien, S. Copper oxide nanocrystals. *J. Am. Chem. Soc.* **2005**, *127*, 9506–9511. [[CrossRef](#)]
26. Goh, S.W.; Buckley, A.N.; Lamb, R.N.; Rosenberg, R.A.; Moran, D. The oxidation states of copper and iron in mineral sulfides, and the oxides formed on initial exposure of chalcopyrite and bornite to air. *Geochim. Cosmochim. Acta* **2006**, *70*, 2210–2228. [[CrossRef](#)]
27. Peng, H.; Wu, D.; Abdelmonem, M. Flotation performances and surface properties of chalcopyrite with xanthate collector added before and after grinding. *Results Phys.* **2017**, *7*, 3567–3573. [[CrossRef](#)]
28. Ghahremaninezhad, A.; Dixon, D.G.; Asselin, E. Electrochemical and XPS analysis of chalcopyrite (CuFeS₂) dissolution in sulfuric acid solution. *Electrochim. Acta* **2013**, *87*, 97–112. [[CrossRef](#)]
29. Klauber, C.; Parker, A.; van Bronswijk, W.; Watling, H. Sulphur speciation of leached chalcopyrite surfaces as determined by X-ray photoelectron spectroscopy. *Int. J. Miner. Process.* **2001**, *62*, 65–94. [[CrossRef](#)]
30. Liu, D.; Zhang, G.; Liu, J.; Pan, G.; Chen, Y.; Wang, M. Studies on the surface oxidation and its role in the flotation of mixed Cu-Ni sulfide ore. *Powder Technol.* **2021**, *381*, 576–584. [[CrossRef](#)]
31. Zhang, Y.; Qin, W.L.; Sun, W.; He, G.Y. Electrochemical behaviors of pyrite flotation using lime and sodium hydroxide as depressants. *Chin. J. Nonferrous Met.* **2011**, *21*, 675–679.
32. Zhao, C.; Wu, B.; Chen, J. Electronic structure and flotation behavior of monoclinic and hexagonal pyrrhotite. *J. Cent. South Univ.* **2015**, *22*, 466–471. [[CrossRef](#)]
33. Yan, H. *Study on the Microthermokinetic of Inhibition and Activation Process of Chalcopyrite*; Jiangxi University of Science and Technology: Ganzhou, China, 2016. [[CrossRef](#)]

Disclaimer/Publisher's Note: The statements, opinions and data contained in all publications are solely those of the individual author(s) and contributor(s) and not of MDPI and/or the editor(s). MDPI and/or the editor(s) disclaim responsibility for any injury to people or property resulting from any ideas, methods, instructions or products referred to in the content.